

# From quantum alchemy to Hammett's equation: Covalent bonding from atomic energy partitioning

Michael J. Sahre,<sup>1, 2</sup> Guido Falk von Rudorff,<sup>1</sup> and O. Anatole von Lilienfeld<sup>3, 4, 5, \*</sup>

<sup>1</sup> University of Vienna, Faculty of Physics, Kolingasse 14-16, 1090 Vienna, Austria

<sup>2</sup> University of Vienna, Vienna Doctoral School in Chemistry (DoSChem), Währinger Str. 42, 1090 Vienna, Austria.

<sup>3</sup> Vector Institute for Artificial Intelligence, Toronto, ON, M5S 1M1, Canada

<sup>4</sup> Departments of Chemistry, Materials Science and Engineering, and Physics, University of Toronto, St. George Campus, Toronto, ON, Canada

<sup>5</sup> Machine Learning Group, Technische Universität Berlin and Institute for the Foundations of Learning and Data, 10587 Berlin, Germany

We present an intuitive and general analytical approximation estimating the energy of covalent single and double bonds between participating atoms in terms of their respective nuclear charges with just three parameters,  $[E_{AB} \approx a - bZ_A Z_B + c(Z_A^{7/3} + Z_B^{7/3})]$ . The functional form of our expression models an alchemical atomic energy decomposition between participating atoms A and B. After calibration, reasonably accurate bond energy estimates are obtained for hydrogen-saturated diatomics composed of *p*-block elements coming from the same row  $2 \leq n \leq 4$  in the periodic table. Corresponding changes in bond energies due to substitution of atom B by C can be obtained via simple formulas. While being of different functional form and origin, our model is as simple and accurate as Pauling's well-known electronegativity model. Analysis indicates that the model's response in covalent bonding to variation in nuclear charge is near-linear—which is consistent with Hammett's equation.

## I. INTRODUCTION

Due to their direct link to thermodynamics stability, computational predictions of binding trends among molecules and materials have greatly improved design choices in the chemical sciences.<sup>1–8</sup> Unfortunately, while numerical bonding estimates obtained from modern and computationally demanding quantum methods are very accurate and predictive, they are at the same time difficult to grasp with human intuition due to the inherent complexity of their solutions to the electronic Schrödinger equation.<sup>9</sup> Already very approximate models, however, can yield intuitive descriptions of important bonding features. For example, Lewis' simple concept of binding electron pairs, in conjunction with the Aufbau principle, imposes relevant constraints from Pauli's exclusion principle,<sup>10</sup> or the delocalization of  $\pi$ -electrons can be easily understood within Hückel theory (FIG 1, left).<sup>11</sup> Pauling's model for covalent bond energies is based on the idea to decompose the wavefunction within valence bond theory into ionic and covalent terms, leading to the chemically intuitive concept of electronegativity (FIG 1, center).<sup>12</sup> Because of their universality due to their foundation in quantum mechanics, these basic models are applicable across chemical compound space, and have proven powerful for advancing our understanding of chemistry—despite their approximate nature.

Less approximate and more recently, energy decomposition methods have been introduced to provide a more detailed understanding of chemical bonding. Partitioning of quantum mechanical observables onto the constituting

parts of the quantum many-body system can be done in arbitrarily many ways. Some methods decompose the energy into different physical contributions<sup>13–17</sup>, others partition it onto atoms<sup>18–22</sup>. These methods have for example been useful to explain differences in stability<sup>23,24</sup> or torsional energy profiles<sup>25</sup> across various molecules.

Also within the framework of computational alchemical perturbation density functional theory<sup>22</sup> one can meaningfully quantify the effect of different binding partners on the atomic energy of every atom in the system<sup>26</sup>. Here, we introduce a model of covalent bonding which we compare to molecular orbital (MO) and valence bond (VB) theory in FIG 1. The model directly emerges from quantum alchemy (QA) based atomic energy decomposition arguments. It is, to the best of our knowledge new, yet as simple and accurate as Pauling's electronegativity model and of a distinctly different functional form and origin. We thus believe that it enables a fresh and intuitive perspective on covalent bonding.

Within quantum alchemy (alchemical perturbation density functional theory<sup>22</sup>) the energy of any molecule  $E^{\text{tot}}$  can be referenced to the uniform electron gas  $E^{\text{UEG}}$  via alchemical thermodynamic integration<sup>26,30,31</sup>. Using the Hellmann-Feynman theorem<sup>32</sup> and the chain-rule affords a formally exact atomic energy  $E_I$  partitioning with respect to nuclear charges,<sup>26</sup>,

$$E^{\text{tot}} - E^{\text{UEG}} = \sum_I Z_I \underbrace{\left( \int d\mathbf{r} \frac{\int_0^1 d\lambda \rho(\lambda, \mathbf{r})}{|\mathbf{r} - \mathbf{R}_I|} + \frac{1}{2} \sum_J \frac{Z_J}{|\mathbf{R}_J - \mathbf{R}_I|} \right)}_{:= E_I}, \quad (1)$$

with  $\rho(\lambda, \mathbf{r})$ ,  $Z_I$ , and  $\mathbf{R}_I$  corresponding to the electron density, the nuclear charge, and the position of the nucleus, respectively.

\* anatole.vonlilienfeld@utoronto.ca

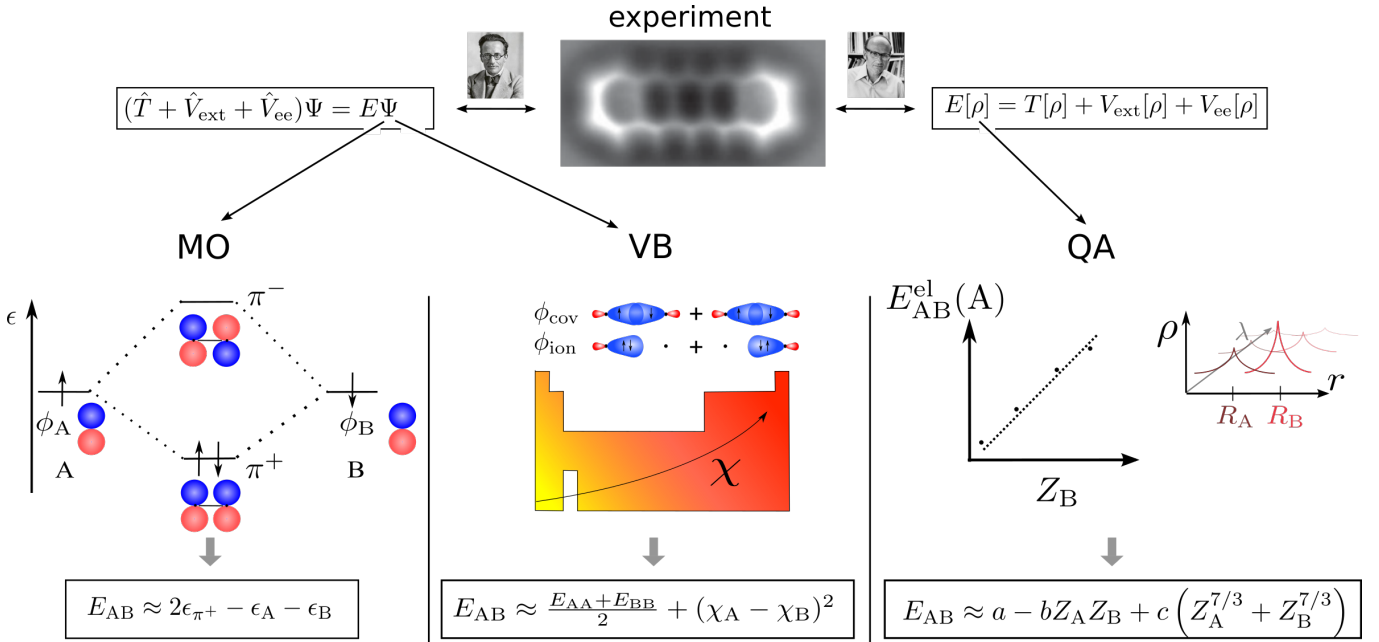


FIG. 1. Experimental measurements (illustrated by atomic force microscopy image of pentacene molecule<sup>27</sup>) inform exact theory (Schrödinger equation & density functional theory) which informs three intuitive approximate views of the chemical bond (MO, VB, QA) in chemical compound space. MO represents molecular orbital theory accounting for bonding in energy diagrams (left). VB corresponds to valence bond theory enabling the decomposition of the wavefunction into covalent and ionic parts (mid). Quantum Alchemy (QA) enables direct partitioning into atomic energies based on thermodynamic integration over varying nuclear charges. MO, VB, and QA can be used to account for bonding trends.<sup>28,29</sup>

Application of our alchemical decomposition scheme to binding energies between *p*-block elements reveals simple dependencies of atomic binding contributions on nuclear charges. This has motivated us to introduce the following approximate Ansatz for the binding energy  $E_{AB}$  between atoms A and B,

$$E_{AB} \approx \underbrace{a}_{\text{period's offset}} - b \underbrace{Z_A Z_B}_{\propto \text{nuc. rep.}} + c \underbrace{(Z_A^{7/3} + Z_B^{7/3})}_{\propto \text{free atoms}}, \quad (2)$$

with simple interpretation for each term and requiring just three global parameters  $a, b, c$ , which effectively account for interatomic distance and bond order (see Methods A for details).

After calibration of parameters, we find that this simple model reproduces covalent binding among *p*-block elements of either the second, third, or fourth row of the periodic table reasonably well. In the following we also analyse and compare the model to density functional theory, quantum machine learning, semi-empirical and post-Hartree-Fock quantum mechanics, Pauling's electronegativity model, and Hammett's equation. We subsequently discuss limitations, extensions to double bonds and different electronic configurations and formulate a generalized expression that predicts bonding trends across multiple periods.

## II. RESULTS AND DISCUSSION

### A. Performance

After regression of parameters to DFT reference data, our model (Eq. (2)) makes surprisingly accurate estimates. In particular, FIG. 2 shows calculated bond dissociation energies (BDEs) for homolytic cleavage of diatomics A-B saturated with Hydrogens,



Here, atoms A and B are fourth to seventh main group elements, both of either second, third or fourth row of the periodic table. BDEs for calibration were obtained from density functional theory (see Computational Details) and the row dependent model parameters were determined from a least-square fit to the ten diatomics in each row (see TABLE I). The residual deviation of estimated binding energies from the DFT reference amounts to an overall mean absolute error (MAE) of just 1.8 kcal/mol across all rows, falling just short of the highly coveted 'chemical accuracy' threshold of  $\sim 1$  kcal/mol. While such accuracy is extremely promising for such a simple functional form and so few parameters, we note the severe restrictions and limitations including fixed effective equilibrium geometries, participating elements, or bond orders.

To set this performance into a wider perspective we

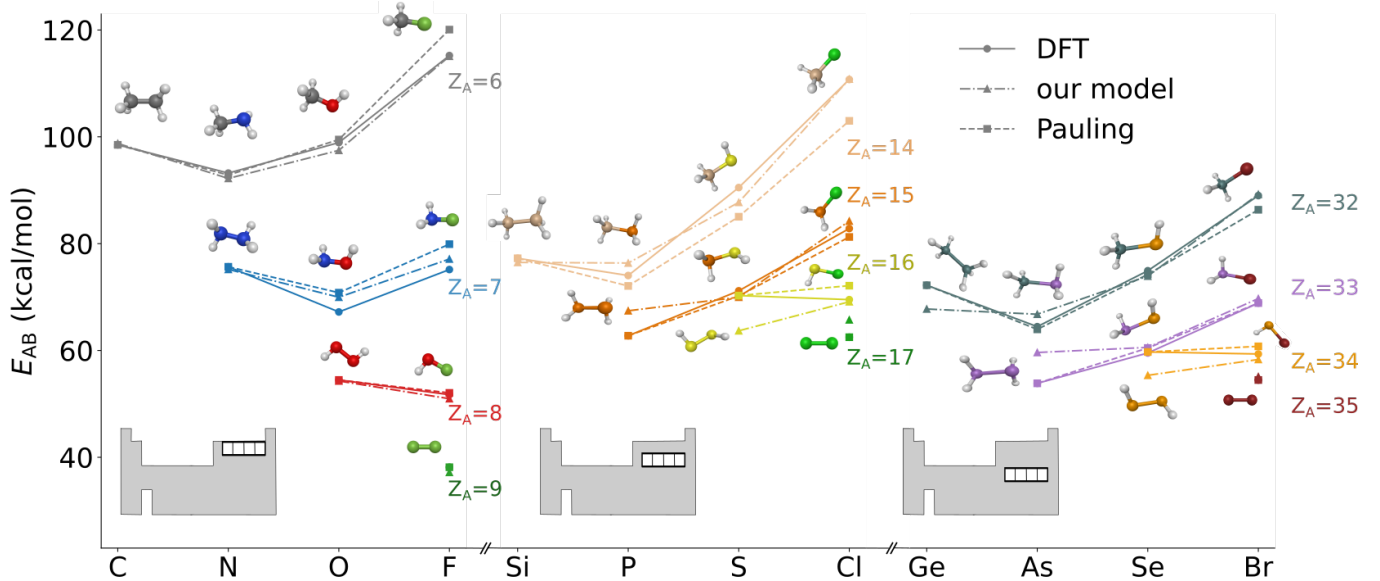


FIG. 2. Calculated bond dissociation energies from density functional theory (DFT, PBE0/def2-TZVP), our quantum alchemy based chemical bond model (Eq. (2)), and Pauling’s electronegativity model in Eq. (4). MAEs with respect to DFT amount to 1.8 and 1.4 kcal/mol for our and Pauling’s model, respectively.

TABLE I. Coefficients and MAEs of our model Eq. (2) for different rows  $n$ .  $b$  is scaled such that  $bZ_AZ_B$  is given in kcal/mol if  $Z_A$  and  $Z_B$  are given in atomic units.

$n$	$a$ (kcal/mol)	$b$ ( $630/a_0$ )	$c$ (kcal/mol)	MAE (kcal/mol)
2	215.7	10.470	1.987	1.0
3	392.7	8.823	1.496	2.4
4	1109.2	6.180	0.813	2.2

compare calculated BDEs among other models well established in the literature. For this purpose, we selected all ten single bond diatomics from the second row contained within the legacy quantum chemistry W4-17 dataset<sup>33</sup> which provides highly accurate bond dissociation energies using explicit electron correlation methods for saturated diatomics in the second row. FIG. 3 shows a scatter plot of BDEs obtained from various models. Calibrating our model using the W4-17 data yields a leave-one-out prediction error of 1.3 kcal/mol (see Computational Details). Training a chemically agnostic quantum machine learning<sup>34–36</sup> surrogate model (see computational details) results in a much higher leave-one-out prediction error of 10.4 kcal/mol. By comparison, generic QM methods such as semi-empirical PM7 method<sup>37</sup>, density functional theory (DFT/PBE0/def2-TZVP), and coupled cluster single double perturbative triples F12 calculations, (taken from G2 Ref.<sup>38</sup>) produce MAEs of 9.5, 1.2, and 0.6 kcal/mol, respectively. This indicates that our model can achieve accurate descriptions of trends in chemical compound space. We should caution, however, that our model is biased due to the calibration, and is likely to perform significantly worse for other chemistries.

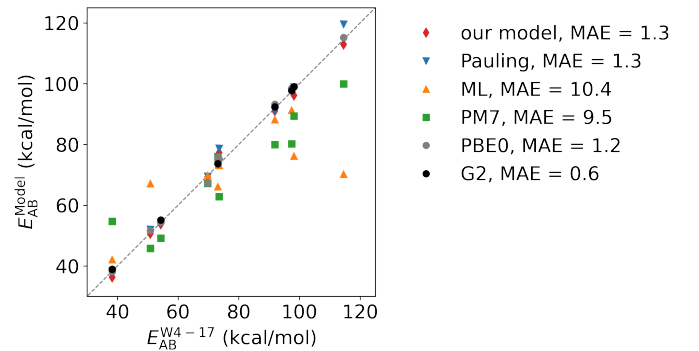


FIG. 3. Calculated BDEs using our model, Pauling’s, various quantum methods (PM7, DFT (PBE0/DEF2-TZVP), G2) and a quantum machine learning model. Binding energies are scattered against the W4 entries<sup>33</sup> for ten saturated single bond diatomics composed of carbon, nitrogen, oxygen or fluorine.

## B. Comparison to Pauling

Pauling’s model and our model are both simple expression with similar overall accuracy. Pauling’s bond model<sup>12</sup> expresses the BDE as

$$E_{AB} = \frac{E_{AA} + E_{BB}}{2} + 23(\chi_A - \chi_B)^2 \quad (4)$$

which depends on the the homolytic binding energies  $E_{AA}$ ,  $E_{BB}$  and the electronegativites  $\chi_A$ ,  $\chi_B$ . The model is based on a wavefunction decomposition into a covalent and an ionic part. Pauling proposed that the bond energy could accordingly be split into a covalent contri-

bution, approximated as the mean of the homolytic bond energies, and an ionic contribution, postulated to be represented by the difference in electronegativities ( $\chi_A - \chi_B$ )<sup>2</sup>. Pauling optimized electronegativities in order to reproduce binding energies as accurately as possible.<sup>12</sup> This model's predictions for our test sets were discussed before (See also FIGs. 2, 3).

Note that Paulings expression requires knowledge of the homolytic bond formation energies and introduces electronegativities as additional quantity while our model relies directly on the nuclear charges. While electronegativity is useful to explain trends in chemical properties, our formulation depending directly on nuclear charges is directly connected to the external potential in the electronic Hamiltonian, and thereby more rigorously rooted in the fundamental physics governing chemistry. Furthermore, homo-diatomics in the third and fourth period dominate the error of our model, while these cases are direct model parameters for Pauling. Note that our model outperforms Pauling's if the binding partners A and B have a large electronegativity difference as observable for example for the C-F, Si-Cl or N-F bond (FIG. 2).

### C. Comparison to Hammett's equation

Another empirical model to quantify property trends across chemical spaces was proposed by Hammett more than 80 years ago<sup>39,40</sup>,

$$P \approx \rho \cdot \sigma. \quad (5)$$

Originally,  $P = \log[K/K_0]$  was the equilibrium constant for various reactions of benzene derivatives normalized with respect to a reference reaction constant  $K_0$ ,  $\sigma$  described the effect of different substituents and  $\rho$  accounted for the reaction type (e.g. mechanism or solvent). However, the model has been used to describe many other properties like activation energies<sup>41</sup>, orbital energies of metal organic complexes<sup>42</sup> or dipole moments<sup>43</sup>. Furthermore, the model has been applied to non-benzyl compounds.<sup>41,44</sup> The relation between Hammett constants and electronegativity has also been noted in the context of nucleo- and electro-philicity relevant for mechanistic discussions in organic chemistry.<sup>45</sup> While Hammett's model is very intuitive since it only requires separability of two dominating variables, its physical motivation has remained unclear.<sup>46</sup>

Our model might offer a rationalization of Hammett's because it emerges from the quantum alchemy based atomic energy decomposition and accounts for the change in binding energy with respect to composition, fully consistent with Hammett's approach. In particular, the change of binding energy with respect to the nuclear charge, the partial derivative of our model, is simply given by

$$\frac{\partial E_{AB}}{\partial Z_B}(Z_A, Z_B) = -bZ_A + \frac{7}{3}cZ_B^{4/3}. \quad (6)$$

FIG. 4 displays the near-linear trend of this derivative for a fixed value of  $Z_A$  as a function of the number of valence electrons  $N_{VE}$  of  $Z_B$  for each period investigated in this study.

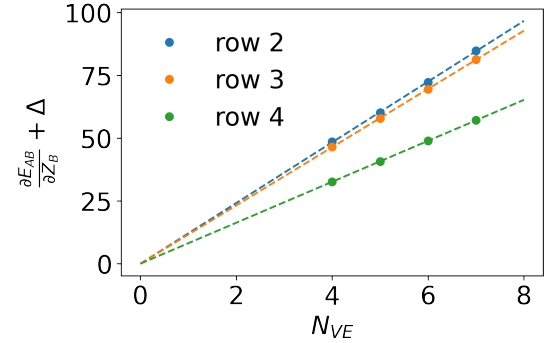


FIG. 4. The sensitivity of the binding energy due to change in composition expressed by a Hammett type relationship between the derivative of the binding energy with respect to the nuclear charge  $\frac{\partial E_{AB}}{\partial Z_B}$  and the number of valence electrons  $N_{VE}$  of binding partner B for binding in different rows of the periodic table. The curves are shifted by a constant  $\Delta$  such that they intersect the origin.

We have shifted each curve by a constant  $\Delta$  such that it intersects the origin at  $N_{VE} = 0$ . The curves are approximately linear in the number of valence electrons with the slopes being proportional to  $\frac{7}{3}c$  (see Eq. (6)). Thus,  $\frac{\partial E_{AB}}{\partial Z_B} + \Delta$  can be modelled by a Hammett ansatz with  $\sigma = N_{VE}$  and  $\rho$  accounting for different binding behaviour due to a change in number of core electrons for different rows. As the row number increases the slope becomes flatter indicating a lower sensitivity of the binding energy to a change of the binding partner as observable in FIG. 2. The drastic decrease of the slope from the third to the fourth row could be due to the additional 10 3d core electrons for elements in the fourth row.

The identification of the number of valence electrons of binding partner B as the  $\sigma$ -parameter is possible because the influence of the binding partner B is expressed as a function of the nuclear charge in our model. We have arrived at this expression based on the atomic energy decomposition within quantum alchemy. We believe that these findings indicate that such decomposition into atomic or fragment contributions can deepen our understanding of empirical rules such as Hammett's model. Note that this finding is also consistent with multiple other studies which found a correlation of the  $\sigma$  parameters with atomic quantities like NMR-shifts<sup>47,48</sup>, polarizing force<sup>49</sup>, fragment self similarity measures<sup>50</sup> or atomic charges<sup>51,52</sup>.

### D. Limitations to covalent bonds

So far, we have only considered typical covalent bonding scenarios between *p*-block elements, i.e. elements from

groups IV-VII in the periodic table. These elements all have in common that their valence electrons share the same second angular momentum quantum number. Our model has not been developed for decreased covalent character, i.e. for bonding atoms with differing second quantum numbers. Not surprisingly, for example, BDEs for single bonds shown in FIG. 5 indicate a qualitatively different behavior when one bonding partner, say atom B, comes from the alkaline or earth-alkaline group. According to our model calibrated for *p* elements only, bond energy content would monotonically increase as the nuclear charge  $Z_B$  decreases. In reality, however, bond energy content must decrease as B changes from predominantly covalent bonding among *p*-block elements into ionic bonding regimes with FF and LiF as the two opposite extremes.

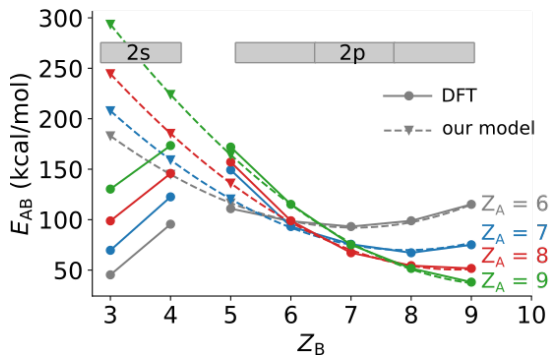


FIG. 5. Limitations of applicability: BDEs between atom A and B corresponding to C/N/O/F or Li/Be/B/C/N/O/F, respectively. For second quantum number differing between A and B, our model [Eq. (2)] breaks down.

### E. Bond order

Close inspection of results for the *p*-block elements shown in FIG. 5 indicates that our model is the least accurate when it comes to the prediction of BDEs involving Boron ( $Z_B = 5$ ). This could be due to the parameters being optimized for bonds with bond orders being close to 1. B-N, B-O and B-F bonds, however, are known to have a bond order of approximately 1.4.<sup>53-55</sup>. Consequently, one should expect our covalent single bond model to systematically underestimate the binding energies for these systems — consistent with the numerical observation.

To further explore this aspect, we have investigated whether our model can be re-calibrated to predict binding energies for other bond orders. We have considered double bonds A=B for all six possible combinations of elements from main groups IV, V and VI within the same row of the periodic table, e.g. carbon, nitrogen and oxygen for the second row. In contrast to the single bonded molecules, the spin state is not the same for all double bonded systems. O<sub>2</sub>, S<sub>2</sub> and Se<sub>2</sub> have triplet ground states while the other molecules are singlets. To remove

the additional complexity due to a change in spin state, we used the same singlet spin state for all double bonded molecules, i.e. we refitted the parameters  $a, b, c$  to energy differences  $\Delta E^{\text{TS}}$  between fragments in a triplet state after homolytic bond cleavage, and the bound molecule in a singlet state. The trend in these binding energies is very similar to the one for single bonds with a decrease in binding energy as the nuclear charges of the binding atom grows. The resulting model's performance is equally good with prediction errors of 0.9, 1.3 and 2.0 kcal/mol for the second, third and fourth row, respectively (see SI with Fig. 11, and TABLE III for optimized parameters).

### F. Electronic configuration

To further investigate the impact of spin, we recalibrated our model to energy differences  $\Delta E^{\text{GS}}$  between the ground states of fragments and molecules, e.g. O<sub>2</sub> in a triplet instead of a singlet state (SI Fig. 12 A, TABLE IV) and the energy differences  $\Delta E^{\text{TT}}$  and  $\Delta E^{\text{SS}}$  with fragments and molecules either both in triplet (SI Fig. 12 B, TABLE V) or both in singlet states (SI Fig. 12 C, TABLE VI). The prediction of  $\Delta E^{\text{GS}}$  yields a MAE of 7.4 kcal/mol for compounds in the second row. This increase in error with respect to  $\Delta E^{\text{TS}}$  could be attributed to mixed spin states of the molecules. However, for the third and fourth row prediction errors for  $\Delta E^{\text{GS}}$  are 1.6 and 1.9 kcal/mol, which is similar to the error for  $\Delta E^{\text{TS}}$ . For these rows, the spin state changes not only for the molecules but also for the fragments. The fourth main group fragments (SiH<sub>2</sub>, GeH<sub>2</sub>) have a singlet ground state while the other fragments are triplets. Thus, changing spin states do not generally lower the accuracy.

The prediction errors for  $\Delta E^{\text{TT}}$  and  $\Delta E^{\text{SS}}$  are around 7-8 kcal/mol for the second row and 10-14 kcal/mol for the third and fourth row (see SI TABLE V and VI for details). The worse performance compared to single bonded systems is not surprising since the functional form of our model is inspired by the alchemical decomposition of bond dissociation energy trends for single bonds in the ground state, that are significantly different from  $\Delta E^{\text{TT}}$  and  $\Delta E^{\text{SS}}$ .

Finally, we have also recalibrated our model (Eq. (2)) to fit randomly drawn points from an uniform distribution in order to assess in how far the performance of our model can be attributed to its mathematical flexibility or rather to its inherent capability to account for the underlying physics of the studied systems (see SI Fig. 13). The MAE of the randomly drawn data is in all cases, except for  $\Delta E^{\text{TT}}$  for the fourth row, substantially higher than for the binding energy differences. This finding corroborates the notion that our model's performance is not coincidence but rather due to its appropriate functional form approximating the relevant physics to a certain degree.

### G. Trends and dependence on period

Since many questions in chemistry only require knowledge about differences in BDEs, we have investigated the applicability of our model towards the prediction of trends among bonds. More specifically, generalization of our model to deal with covalent bonding within *any* row from the *p*-block with just 3 parameters  $a, b, c$  is impossible due to the large differences in nuclear charges with increasing row number  $n$ . We find, however, that  $a, b$ , and  $c$  vary smoothly with  $n$  when predicting changes in BDEs, i.e.  $\Delta E = E_{AB} - E_{AC}$ , in combination with a second order Taylor expansion of the  $Z^{7/3}$ -terms. Then, parameters can be described as simple functions of the principal quantum number  $n$  (the row number) and  $\Delta E$  is approximately given by

$$\Delta E \approx \Delta Z [28(n-1) + (8.5 + (n-3)^2)Z_A] + 6(Z_B^2 - Z_C^2) \quad (7)$$

with the change in nuclear charges  $\Delta Z = Z_C - Z_B$  (see Methods section for details).

Encouragingly, Eq. 7 meaningfully reproduces changes in covalent bond energies covering ranges from -40 to +70 kcal/mol with a MAE of just 4.2 kcal/mol with respect to density functional theory. Results are shown in FIG. 6) for any single bond changes within second, third, or fourth row of the periodic table.

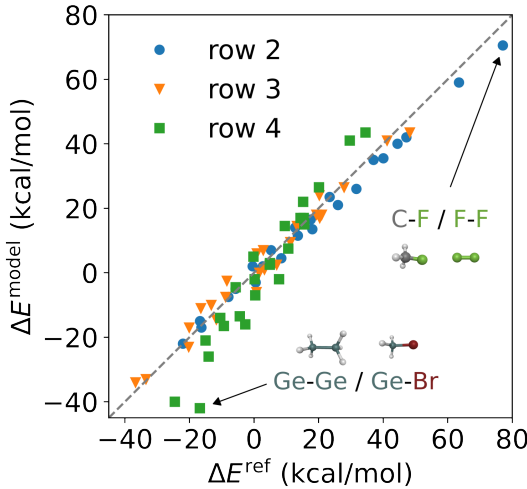


FIG. 6. Trends in covalent binding: Predicted (Eq. (7)) vs. Truth (corresponding to PBE0/def2-TZVP). 72 binding energy differences between bonds A-B and A-C ( $\Delta E$ ), both within either the second, third, or fourth row of the periodic table,  $\Delta E = E_{AB} - E_{AC}$ , where  $Z_B \leq Z_C$ . Corresponding molecules involved are on display in FIG. 2.

Albeit of interest, the generalization of Eq. 7 to also account for atoms A and B and C coming from *different* rows, or to involve other bond-orders, has not yet been explored in this study.

### III. CONCLUSION

We have presented a simple and, to the best of our knowledge, novel expression of covalent bonding in terms of nuclear charges. Despite its simplicity, it is deeply rooted in the underlying physics of quantum mechanics via the computational alchemy based reasoning. The expression might prove useful for developing an improved intuition regarding trends of bonding energies across chemical compound space. It has only three calibration parameters which can easily be regressed to available reference data.

We have found the model to be limited to covalent single and double bonds among atoms with the same first and second quantum number. We have presented promising numerical evidence for *p*-block atoms (except for rare gas elements) coming from 2nd, 3rd, and 4th row. We have compared our model to Pauling's electronegativity model, and we have discussed its consistency with respect to Hammett's equation. We note that the description of ionic, metallic, or van der Waals bonding through inclusion of *s* and *d* block elements is still outstanding and will be part of future research. This also holds for the generalization to bonds involving elements that differ in principal quantum numbers.

Conceptionally speaking, our model relies on coarse-graining the expectation value of the electronic Hamiltonian throughout chemical space. As such, it is consistent with quantum mechanics and offers a fresh perspective on bond dissociation energies which is in line with Hammett's expression. Historically speaking, it represents an equally powerful yet possibly less empirical alternative to Pauling's electronegativity model. Future work will show to which extent this partitioning approach can be used to deepen our understanding of chemical space with respect to other extensive properties, and if it is useful for computational materials and molecular design efforts.

### IV. METHODS

#### A. Construction of the model

Continuing from Eq. (1), the electronic energy  $E^{\text{el}}(\text{AB})$  of a saturated diatomic A-B can be decomposed into

$$\begin{aligned} E^{\text{el}}(\text{AB}) = & E^{\text{el}}(\text{A/AB}) + E^{\text{el}}(\text{B/AB}) \\ & + E^{\text{el}}(\text{AH/AB}) + E^{\text{el}}(\text{BH/AB}) \end{aligned} \quad (8)$$

where  $E^{\text{el}}(\text{A/AB})$  and  $E^{\text{el}}(\text{B/AB})$  are the atomic energies of A and B and  $E^{\text{el}}(\text{AH/AB})$  and  $E^{\text{el}}(\text{BH/AB})$  are the sum of atomic energies of the hydrogens attached to A and B, respectively (see FIG. 7 for an example).

Furthermore, the electronic contribution to the binding energy  $E_{\text{AB}}^{\text{el}}$  is the difference between the electronic energies of the fragments A and B generated by homolytic bond cleavage and the electronic energy of compound AB

$$E_{\text{AB}}^{\text{el}} = E^{\text{el}}(\text{A}) + E^{\text{el}}(\text{B}) - E^{\text{el}}(\text{AB}). \quad (9)$$

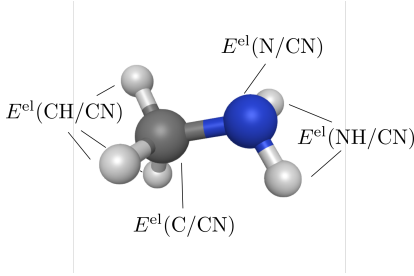


FIG. 7. Atomic electronic energy decomposition notation exemplified for methylamine.

The electronic contribution to the *atomic* binding energy, e.g.  $E_{AB}^{\text{el}}(A)$  for atom A is then defined as

$$E_{AB}^{\text{el}}(A) = E^{\text{el}}(A/A) - E^{\text{el}}(A/AB) \quad (10)$$

where  $E^{\text{el}}(A/A)$  and  $E^{\text{el}}(A/AB)$  are the atomic energies of A in fragment A and diatomic compound AB, respectively.

Calculating such atomic binding energies according to APDFT<sup>26</sup>, we have observed that  $E_{AB}^{\text{el}}(A)$  increases approximately linearly with the nuclear charge  $Z_B$  of binding partner B for saturated diatomics composed from the elements carbon, nitrogen, oxygen and fluorine (SI FIG. 8A). Furthermore, the atomic energy of the hydrogen atoms remains approximately constant with varying binding partner (SI FIG. 8B).

This enables us to express the binding energy approximately as

$$E_{AB}^{\text{el}} \approx \underbrace{\beta_A Z_B + \alpha_A}_{=E_{AB}^{\text{el}}(A) + E_{AB}^{\text{el}}(\text{AH})} + \underbrace{\beta_B Z_A + \alpha_B}_{=E_{AB}^{\text{el}}(B) + E_{AB}^{\text{el}}(\text{BH})}. \quad (11)$$

The energy contributions of fragments A and B are characterized by the parameters  $\alpha_A$ ,  $\beta_A$  and  $\alpha_B$ ,  $\beta_B$ , respectively.  $\alpha$  accounts for the constant contribution of the heavy atom (A or B) and of the hydrogens attached to it to the binding energy, while  $\beta$  describes the contribution of the heavy atom for varying binding partners. Furthermore, we approximate the contribution of the nuclear repulsion to the binding energy  $E_{AB}^{\text{nuc}}$  by only considering the interaction between the heavy atoms A and B at an average bond distance  $\bar{d}$ . This average is calculated from the bond lengths between A and B for all considered compounds A-B. Consequently, the total binding energy  $E_{AB}$  including nuclear repulsion can be expressed as

$$E_{AB} \approx \underbrace{\beta_A Z_B + \alpha_A}_{=E_{AB}^{\text{el}}(A) + E_{AB}^{\text{el}}(\text{AH})} + \underbrace{\beta_B Z_A + \alpha_B}_{=E_{AB}^{\text{el}}(B) + E_{AB}^{\text{el}}(\text{BH})} - \underbrace{\frac{Z_A Z_B}{\bar{d}}}_{=E_{AB}^{\text{nuc}}}. \quad (12)$$

The parameters  $\alpha$ ,  $\beta$  are determined from a least squares fit to  $E_{AB} + \frac{Z_A Z_B}{\bar{d}}$  for all ten unique combinations A-B of carbon, nitrogen, oxygen and fluorine. The binding energies  $E_{AB}$  are calculated with DFT (see Computational Details).

While Eq. (12) is based on trends for diatomics in the second row of the periodic table, we also apply it to diatomics from the fourth to seventh main group of the third and fourth row.

The mean absolute errors (MAEs) for binding energy predictions with Eq. (12) are 0.5, 0.4 and 0.3 kcal/mol for rows 2-4, respectively and the optimized parameters can be found in the SI in TABLE II. The model accurately reproduces the binding energies and can be applied to different rows of the periodic table. However, it is also prone to overfitting because it uses eight parameters to model binding energies for ten compounds. Thus, we studied the relation of the parameters  $\alpha$ ,  $\beta$  on the nuclear charge of the respective element in an attempt to reduce the number of parameters.

The optimized parameter  $\beta_A$  correlates linearly with  $Z_A$

$$\beta_A \approx b' Z_A. \quad (13)$$

as shown in SI FIG. 9A. Thus, the terms  $\beta_A Z_B$  and  $\beta_B Z_A$  in Eq. (12) can be written as

$$\beta_A Z_B + \beta_B Z_A \approx 2b' Z_A Z_B. \quad (14)$$

The  $\beta$ -terms account mainly for the large nuclear repulsion term  $Z_A Z_B d^{-1} \gg E_{AB}$  in the dependent variable  $E_{AB} + \frac{Z_A Z_B}{\bar{d}}$ . We note that the linear dependence of  $\beta_A$  on  $Z_A$  is also consistent with the relation

$$E_{QR}^{\text{el}} \approx E_{SR}^{\text{el}} + \frac{1}{2} (E_{QQ}^{\text{el}} + E_{SS}^{\text{el}}), \quad (15)$$

between binding energies of elements Q, R and S with  $Z_Q = Z_R - 1 = Z_S - 2$ , that was derived from alchemical enantiomers.<sup>56</sup> Insertion of the definition for electronic binding energies from Eq. (11) into Eq. (15) yields

$$\begin{aligned} \beta_Q Z_R + \alpha_Q + \beta_R Z_Q + \alpha_R &= \beta_S Z_R + \alpha_S + \beta_R Z_S + \alpha_R \\ &\quad + \beta_Q Z_Q + \alpha_Q - \beta_S Z_S - \alpha_S \\ \beta_Q Z_R + \beta_R Z_Q &= \beta_S Z_R + \beta_R Z_S + \beta_Q Z_Q - \beta_S Z_S \\ \beta_R \underbrace{(Z_Q - Z_S)}_{=-2} &= \beta_S \underbrace{(Z_R - Z_S)}_{=-1} + \beta_Q \underbrace{(Z_Q - Z_R)}_{=-1} \\ \beta_R &= \frac{\beta_S + \beta_Q}{2}, \end{aligned} \quad (16)$$

which implies a linear relation between the different values for  $\beta$ .

The optimized offset  $\alpha_A$  has a non-linear relationship with  $Z_A$  (SI FIG. 9B). Thus, we model the dependence of  $\alpha_A$  on  $Z_A$  as

$$\alpha_A \approx c Z_A^\gamma + a', \quad (17)$$

where the exponent  $\gamma$  accounts for the non-linearity.

Substitution of  $\beta$  and  $\alpha$  in Eq. (12) with the expressions in Eq. (13) and Eq. (17) and rearrangement of the resulting equation yields

$$E_{AB} \approx a - b Z_A Z_B + c (Z_A^\gamma + Z_B^\gamma) \quad (18)$$

with  $a = 2a'$  and  $b = (\frac{1}{d} - 2b')$ . Optimization of the parameters in Eq. (18) by a combination of non-linear least squares for  $a, b, c$  and a line scan for  $\gamma$  leads to similar values for the optimal exponent  $\gamma_{\text{opt}}$  for the different rows (see SI FIG. 10). Thus,  $\gamma$  is kept the same for all rows and only  $a, b, c$  are optimized for each row independently. The optimal value for  $\gamma$  in this optimization procedure is  $\gamma_{\text{opt}} = 2.36 \approx \frac{7}{3}$ . This is an interesting result because  $-0.768745 \cdot Z^{7/3}$  is the leading term in an expansion of the energy of a free atom in its nuclear charge.<sup>57,58</sup> Hence, the binding energy can be expressed as

$$\begin{aligned} E_{AB} &\approx a - bZ_A Z_B + c \left( Z_A^{7/3} + Z_B^{7/3} \right) \\ &\approx a - bZ_A Z_B + c' (E_A^{\text{atom}} + E_B^{\text{atom}}) \end{aligned} \quad (19)$$

with the energies of the free atoms  $E_A^{\text{atom}}$  and  $E_B^{\text{atom}}$  and  $c' = -\frac{c}{0.768745}$ .

### B. Arriving at Eq. (7)

The  $Z^{7/3}$  terms in our model can be approximated by a second order Taylor expansion as

$$Z^{7/3} \approx Z_0^{7/3} + \frac{7}{3} Z_0^{4/3} (Z - Z_0) + \frac{14}{9} Z_0^{1/3} (Z - Z_0)^2 \quad (20)$$

with  $Z_0$  being a suitable reference nuclear charge. Insertion of this expression into our model leads to

$$\begin{aligned} E_{AB} &= a - bZ_A Z_B \\ &+ c \left( \underbrace{\frac{4}{9} Z_0^{7/3}}_{=\xi} - \underbrace{\frac{7}{9} Z_0^{4/3}}_{=\eta} (Z_A + Z_B) + \underbrace{\frac{14}{9} Z_0^{1/3}}_{=\mu} (Z_A^2 + Z_B^2) \right) \\ &= a + \underbrace{\frac{4}{9} Z_0^{7/3} c}_{=\xi} - \underbrace{\frac{7}{9} Z_0^{4/3} c}_{=\eta} (Z_A + Z_B) \\ &- bZ_A Z_B + \underbrace{\frac{14}{9} Z_0^{1/3} c}_{=\mu} (Z_A^2 + Z_B^2). \end{aligned} \quad (21)$$

The quadratic terms can be written as

$$\begin{aligned} Z_A^2 + Z_B^2 &= Z_A^2 + Z_B^2 + 2Z_A Z_B - Z_A Z_B \\ &= (Z_A - Z_B)^2 + 2Z_A Z_B \end{aligned} \quad (22)$$

leading to

$$\begin{aligned} E_{AB} &= \xi - \eta (Z_A + Z_B) - bZ_A Z_B \\ &+ \mu ([Z_A - Z_B]^2 + 2Z_A Z_B) \\ &= \xi - \eta (Z_A + Z_B) + (2\mu - b) Z_A Z_B \\ &+ \mu (Z_A - Z_B)^2. \end{aligned} \quad (23)$$

The energy differences  $\Delta E = E_{AB} - E_{AC}$  between A-B and A-C is then

$$\begin{aligned} \Delta E &= -\eta (Z_B - Z_C) + \kappa Z_A (Z_B - Z_C) \\ &+ \mu ((Z_A - Z_B)^2 - (Z_A - Z_C)^2) \end{aligned} \quad (24)$$

with  $\kappa = (2\mu - b)$ .

To account for the dependence of  $\eta, \kappa$  and  $\mu$  on the row or principal quantum number  $n$  we make the ansatz  $\eta = \tilde{\eta}(n-1)$ ,  $\kappa = (n-3)^2 - \tilde{\kappa}$ , while we choose  $\mu$  to be independent from the principal quantum number. Non-linear least squares optimization of  $\tilde{\eta}$ ,  $\tilde{\kappa}$  and  $\mu$  with respect to  $\Delta E$  in the resulting expression

$$\begin{aligned} \Delta E &= -\tilde{\eta}(n-1) (Z_B - Z_C) \\ &+ [(n-3)^2 - \tilde{\kappa}] Z_A (Z_B - Z_C) \\ &+ \mu ((Z_A - Z_B)^2 - (Z_A - Z_C)^2). \end{aligned} \quad (25)$$

gives  $\tilde{\eta} = 28$ ,  $\tilde{\kappa} = 8.5$  and  $\mu = 6$ , so that

$$\begin{aligned} \Delta E &= -28(n-1) (Z_B - Z_C) \\ &- [8.5 + (n-3)^2] Z_A (Z_B - Z_C) \\ &+ 6 ((Z_A - Z_B)^2 - (Z_A - Z_C)^2) \end{aligned} \quad (26)$$

or alternatively

$$\begin{aligned} \Delta E &= -28(n-1) \Delta Z - (8.5 + (n-3)^2) Z_A \Delta Z \\ &+ 6 (Z_B^2 - Z_C^2) \end{aligned} \quad (27)$$

with  $\Delta Z = Z_B - Z_C$ .

## V. COMPUTATIONAL DETAILS

The atomic energies (Eq. (1)) of the saturated diatomics were calculated using geometries from the amons dataset<sup>59</sup>. The fragment structures were generated by splitting the homo-diatomics without further geometry optimization. The required electron densities were obtained following the procedure in earlier work<sup>26</sup> from calculations with the CPMD<sup>60</sup> code and the CPMD2CUBE program<sup>61</sup> using the PBE<sup>62</sup> functional in a plane wave basis with a cutoff of 200 Ryd, GTH<sup>63,64</sup> pseudopotentials and a wavefunction gradient convergence set to  $10^{-6}$ . A primitive cell with a box length of 14.338 Å was used for saturated diatomics and of 11.380 Å for the fragments. The GTH pseudopotential parameters were scaled by  $\lambda = 6/14, 8/14, 11/14, 1$  and  $\lambda = 3/7, 4/7, 6/7, 1$  for the saturated diatomics and the fragments, respectively to generate electron densities for different values of  $\lambda$ . The electron density at  $\lambda = 0$  was represented as a uniform distribution. The integration with respect to  $\mathbf{r}$  and  $\lambda$  was carried out as weighted summation over grid points and with the trapezoidal rule, respectively.

The binding energies to determine the optimal parameters in Eq. (2) and (12) were calculated with PySCF<sup>65-68</sup> for single bonded systems and with GAUSSIAN<sup>69</sup> for double bonded systems with PBE0/def2-TZVP<sup>70</sup> (restricted open shell for fragments). Reported binding energies are for optimized geometries of saturated diatomics and fragments. Initial guesses for the structures were

generated through the LERULI API<sup>71–74</sup>. The parameter optimization in Eq. (2), (7), (12), (18) was performed by linear or non-linear least squares fitting as implemented in numpy<sup>75</sup> and scipy<sup>76</sup>. Binding energies of our model presented in FIG. 3 are with respect to W4-17 data after determining the parameters via leave-one-out crossvalidation. The machine learning predictions were obtained from kernel ridge regression with a Gaussian kernel and the bag of bonds<sup>77</sup> representation in leave-one-out crossvalidation. Predictions with Paulings model Eq. (4) use electronegativities as reported by Pauling<sup>12</sup>.

## A. Data

The binding energies, example input files and pseudopotentials to calculate alchemical atomic energies and code used to optimize the parameters in the different versions of our model are available at [https://github.com/michasahre/bonding\\_from\\_alchemy](https://github.com/michasahre/bonding_from_alchemy).

## ACKNOWLEDGEMENTS

We acknowledge discussions with M. Meuwly, M. Bragato and P. Marquetand, as well as support from the European Research Council (ERCCoG Grant QML). This project has received funding from the European Union’s Horizon 2020 research and innovation programme under Grant Agreement #772834.

---

[1] O. A. von Lilienfeld, Towards the Computational Design of Compounds from First Principles, in *Many-Electron Approaches in Physics, Chemistry and Mathematics: A Multidisciplinary View*, edited by V. Bach and L. D. Site (Springer Cham, 2014) pp. 169–189.

[2] B. Honarpourvar, T. Govender, G. E. Maguire, M. E. Soliman, and H. G. Kruger, Integrated approach to structure-based enzymatic drug design: Molecular modeling, spectroscopy, and experimental bioactivity, *Chemical Reviews* **114**, 493 (2014).

[3] H. M. Kumalo, S. Bhakat, and M. E. Soliman, Theory and applications of covalent docking in drug discovery: Merits and pitfalls, *Molecules* **20**, 1984 (2015).

[4] N. London, R. M. Miller, S. Krishnan, K. Uchida, J. J. Irwin, O. Eidam, L. Gibold, P. Cimermančič, R. Bonnet, B. K. Shoichet, and J. Taunton, Covalent docking of large libraries for the discovery of chemical probes, *Nature chemical biology* **10**, 1066 (2014).

[5] J. K. Nørskov, T. Bligaard, J. Rossmeisl, and C. H. Christensen, Towards the computational design of solid catalysts, *Nature Chemistry* **1**, 37 (2009).

[6] S. Curtarolo, G. L. Hart, M. B. Nardelli, N. Mingo, S. Sanvito, and O. Levy, The high-throughput highway to computational materials design, *Nature Materials* **12**, 191 (2013).

[7] R. T. Hannagan, G. Giannakakis, R. Réocreux, J. Schumann, J. Finzel, Y. Wang, A. Michaelides, P. Deshlahra, P. Christopher, M. Flytzani-Stephanopoulos, M. Stamatakis, and E. C. H. Sykes, First-principles design of a single-atom-alloy propane dehydrogenation catalyst, *Science* **372**, 1444 (2021).

[8] D. Schwalbe-Koda, S. Kwon, C. Paris, E. Bello-Jurado, Z. Jensen, E. Olivetti, T. Willhammar, A. Corma, Y. Román-Leshkov, M. Moliner, and R. Gómez-Bombarelli, A priori control of zeolite phase competition and intergrowth with high-throughput simulations, *Science* **374**, 308 (2021).

[9] T. Helgaker, P. Jørgensen, and J. Olsen, *Molecular Electronic-Structure Theory* (John Wiley & Sons, Ltd, 2000).

[10] L. Zhao, W. H. Schwarz, and G. Frenking, The Lewis electron-pair bonding model: the physical background, one century later, *Nature Reviews Chemistry* **3**, 35 (2019).

[11] E. Hückel, Quantentheoretische Beiträge zum Benzolproblem, *Zeitschrift für Physik* **70**, 204 (1932).

[12] L. Pauling, *The Nature of the Chemical Bond* (Cornell University Press, 1960) pp. 79–96.

[13] K. Morokuma, Molecular Orbital Studies of Hydrogen Bonds. III. C=O–H–O Hydrogen Bond in H<sub>2</sub>CO–H<sub>2</sub>O and H<sub>2</sub>CO–2H<sub>2</sub>O, *The Journal of Chemical Physics* **55**, 1236 (1971), <https://doi.org/10.1063/1.1676210>.

[14] T. Ziegler and A. Rauk, On the calculation of bonding energies by the Hartree Fock Slater method - I. The transition state method, *Theoretica Chimica Acta* **46**, 1 (1977).

[15] G. Frenking and F. Matthias Bickelhaupt, The EDA Perspective of Chemical Bonding, in *The Chemical Bond* (John Wiley & Sons, Ltd, 2014) Chap. 4, pp. 121–157.

[16] M. Rahm and R. Hoffmann, Toward an experimental quantum chemistry: Exploring a new energy partitioning, *Journal of the American Chemical Society* **137**, 10282 (2015).

[17] B. Zulueta, S. V. Tulyani, P. R. Westmoreland, M. J. Frisch, E. J. Petersson, G. A. Petersson, and J. A. Keith, A Bond-Energy/Bond-Order and Populations Relationship, *Journal of Chemical Theory and Computation* **18**, 4774 (2022), pMID: 35849729.

[18] J. M. Guevara-Vela, E. Francisco, T. Rocha-Rinza, and A. Martín Pendás, Interacting Quantum Atoms-A Review, *Molecules* **25**, 10.3390/molecules25174028 (2020).

[19] M. Yu, D. R. Trinkle, and R. M. Martin, Energy density in density functional theory: Application to crystalline defects and surfaces, *Phys. Rev. B* **83**, 115113 (2011).

[20] V. Barone and S. Fliszár, Theoretical energies of representative carbon-carbon bonds, *International Journal of Quantum Chemistry* **55**, 469 (1995).

[21] J. J. Eriksen, Mean-field density matrix decompositions, *Journal of Chemical Physics* **153**, 10.1063/5.0030764 (2020), arXiv:2009.10837.

[22] G. F. von Rudorff and O. A. von Lilienfeld, Alchemical perturbation density functional theory, *Physical Review*

Research **2**, 23220 (2020).

[23] E. Blokker, X. Sun, J. Poater, J. M. van der Schuur, T. A. Hamlin, and F. M. Bickelhaupt, The Chemical Bond: When Atom Size Instead of Electronegativity Difference Determines Trend in Bond Strength, *Chemistry - A European Journal* **3**, 1 (2021).

[24] T. Hansen, P. Vermeeren, F. M. Bickelhaupt, and T. A. Hamlin, Stability of alkyl carbocations, *Chemical Communications* **58**, 12050 (2022).

[25] M. G. Darley and P. L. Popelier, Role of short-range electrostatics in torsional potentials, *Journal of Physical Chemistry A* **112**, 12954 (2008).

[26] G. F. Von Rudorff and O. A. Von Lilienfeld, Atoms in Molecules from Alchemical Perturbation Density Functional Theory, *Journal of Physical Chemistry B* **123**, 10073 (2019), arXiv:1907.06677.

[27] L. Gross, F. Mohn, N. Moll, P. Liljeroth, and G. Meyer, The Chemical Structure of a Molecule Resolved by Atomic Force Microscopy, *Science* **325**, 1110 (2009).

[28] [https://austria-forum.org/af/Wissenssammlungen/Essays/Naturwissenschaften/Auf\\_der\\_Suche\\_nach\\_dem\\_Leben\\_%28Erwin\\_Schr%C3%BDdinger%29](https://austria-forum.org/af/Wissenssammlungen/Essays/Naturwissenschaften/Auf_der_Suche_nach_dem_Leben_%28Erwin_Schr%C3%BDdinger%29), last accessed 10.04.2022 15:55, ©Wiener Zeitung/Bettmann/CORBIS.

[29] <https://physicstoday.scitation.org/do/10.1063/pt.6.6.20180309a/full/>, last accessed 10.04.2022 16:03, Photo credit: Bill Brooks, AIP Emilio Segrè Visual Archives, Physics Today Collection.

[30] E. B. Wilson, Four-dimensional electron density function, *The Journal of Chemical Physics* **36**, 2232 (1962).

[31] O. A. Von Lilienfeld, First principles view on chemical compound space: Gaining rigorous atomistic control of molecular properties, *International Journal of Quantum Chemistry* **113**, 1676 (2013), arXiv:1209.5033.

[32] R. P. Feynman, Forces in Molecules, *Phys. Rev.* **56**, 340 (1939).

[33] A. Karton, N. Sylvestsky, and J. M. Martin, W4-17: A diverse and high-confidence dataset of atomization energies for benchmarking high-level electronic structure methods, *Journal of Computational Chemistry* **38**, 2063 (2017).

[34] B. Huang and O. A. Von Lilienfeld, Ab Initio Machine Learning in Chemical Compound Space, *Chemical Reviews* **121**, 10001 (2021), arXiv:2012.07502.

[35] A. Tkatchenko, Machine learning for chemical discovery, *Nature Communications* **11**, 8 (2020).

[36] O. A. von Lilienfeld, K. R. Müller, and A. Tkatchenko, Exploring chemical compound space with quantum-based machine learning, *Nature Reviews Chemistry* **4**, 347 (2020), arXiv:1911.10084.

[37] J. Stewart, Optimization of parameters for semiempirical methods VI: more modifications to the NDDO approximations and re-optimization of parameters., *J. Mol. Model.* **19**, 1 (2013).

[38] R. Haunschmid and W. Klopper, New accurate reference energies for the G2/97 test set, *Journal of Chemical Physics* **136**, 10.1063/1.4704796 (2012).

[39] L. P. Hammett, The Effect of Structure upon the Reactions of Organic Compounds. Benzene Derivatives, *Journal of the American Chemical Society* **59**, 96 (1937).

[40] L. P. Hammett, The Effect of Structure upon the Reactions of Organic Compounds. Benzene Derivatives, *Journal of the American Chemical Society* **59**, 96 (1937).

[41] M. Bragato, G. F. Von Rudorff, and O. A. Von Lilienfeld, Data enhanced Hammett-equation: Reaction barriers in chemical space, *Chemical Science* **11**, 11859 (2020).

[42] A. M. Chang, J. G. Freeze, and V. S. Batista, Hammett neural networks: prediction of frontier orbital energies of tungsten-benzylidyne photoredox complexes, *Chem. Sci.* **10**, 6844 (2019).

[43] L. K. H. van Beek, *Recl. Trav. Chim. Pays-Bas* **76**, 729 (1957).

[44] M. Ayoubi-Chianeh and M. Z. Kassaei, Toward triplet disilavinylenes: A Hammett electronic survey for substituent effects on singlet-triplet energy gaps of silylenes by DFT, *Journal of Physical Organic Chemistry* **32**, e3988 (2019), e3988 POC-19-0058.R1, <https://onlinelibrary.wiley.com/doi/pdf/10.1002/poc.3988>.

[45] L. Liu, Y. Fu, R. Liu, R.-Q. Li, and Q.-X. Guo, Hammett Equation and Generalized Pauling's Electronegativity Equation, *Journal of Chemical Information and Computer Sciences* **44**, 652 (2004), pMID: 15032547, <https://doi.org/10.1021/ci0342122>.

[46] I. Fernández and G. Frenking, Correlation between Hammett Substituent Constants and Directly Calculated  $\pi$ -Conjugation Strength, *The Journal of Organic Chemistry* **71**, 2251 (2006), pMID: 16526770, <https://doi.org/10.1021/jo052012e>.

[47] C. H. Yoder, R. H. Tuck, and R. E. Hess, Nuclear magnetic resonance studies of the bonding in aromatic systems. Correlation of Hammett sigma constants with methyl  $^{13}\text{C}$ -H coupling constants and chemical shifts, *Journal of the American Chemical Society* **91**, 539 (1969).

[48] T. Axenrod, P. S. Pregosin, M. J. Wieder, and G. W. A. Milne, Nitrogen-15 magnetic resonance spectroscopy. Correlation of the  $^{15}\text{N}$ -H coupling constants in aniline derivatives with Hammett  $\sigma$  constants, *Journal of the American Chemical Society* **91**, 3681 (1969).

[49] C. C. Price, Substitution and Orientation in the Benzene Ring., *Chemical Reviews* **29**, 37 (1941).

[50] X. Gironés and R. Ponec, Molecular Quantum Similarity Measures from Fermi Hole Densities: Modeling Hammett Sigma Constants, *Journal of Chemical Information and Modeling* **46**, 1388 (2006), pMID: 16711758.

[51] P. Genix, H. Jullien, and R. Le Goas, Estimation of Hammett sigma constants from calculated atomic charges using partial least squares regression, *Journal of Chemometrics* **10**, 631 (1996).

[52] P. Ertl, Simple Quantum Chemical Parameters as an Alternative to the Hammett Sigma Constants in QSAR Studies, *Quantitative Structure-Activity Relationships* **16**, 377 (1997).

[53] I. Mayer, Charge, bond order and valence in the AB initio SCF theory, *Chemical Physics Letters* **97**, 270 (1983).

[54] I. Mayer, Bond order and valence: Relations to Mulliken's population analysis, *International Journal of Quantum Chemistry* **26**, 151 (1984), <https://onlinelibrary.wiley.com/doi/pdf/10.1002/qua.560260111>.

[55] A. J. Bridgeman, G. Cavigliasso, L. R. Ireland, and J. Rothery, The Mayer bond order as a tool in inorganic chemistry, *J. Chem. Soc., Dalton Trans.*, 2095 (2001).

[56] G. F. Von Rudorff and O. Anatole von Lilienfeld, Simplifying inverse materials design problems for fixed lattices with alchemical chirality, *Science Advances* **7**, 1 (2021).

[57] J. Scott, LXXXII. The binding energy of the Thomas-Fermi Atom, *The London, Edinburgh, and Dublin Philo-*

sophical Magazine and Journal of Science **43**, 859 (1952).

[58] J. Schwinger, Thomas-Fermi model: The leading correction, *Phys. Rev. A* **22**, 1827 (1980).

[59] B. Huang and O. A. von Lilienfeld, Quantum machine learning using atom-in-molecule-based fragments selected on the fly, *Nature Chemistry* **12**, 945 (2020), 1707.04146.

[60] Copyright IBM Corp. 1990-2019 and Copyright MPI-FKF Stuttgart 1997-2001, CPMD 4.3, <http://www.cpmd.org>.

[61] Silvestri, Walter and Seitsonen, Ari P. and Boero, Mauro and Kohlmeyer, Axel, CPMD2CUBE, <http://www.cpmd.org>.

[62] J. P. Perdew, K. Burke, and M. Ernzerhof, Generalized Gradient Approximation Made Simple, *Phys. Rev. Lett.* **77**, 3865 (1996).

[63] S. Goedecker, M. Teter, and J. Hutter, Separable dual-space Gaussian pseudopotentials, *Phys. Rev. B* **54**, 1703 (1996).

[64] C. Hartwigsen, S. Goedecker, and J. Hutter, Relativistic separable dual-space Gaussian pseudopotentials from H to Rn, *Phys. Rev. B* **58**, 3641 (1998).

[65] Q. Sun, X. Zhang, S. Banerjee, P. Bao, M. Barbry, N. S. Blunt, N. A. Bogdanov, G. H. Booth, J. Chen, Z.-H. Cui, J. J. Eriksen, Y. Gao, S. Guo, J. Hermann, M. R. Hermes, K. Koh, P. Koval, S. Lehtola, Z. Li, J. Liu, N. Mardirossian, J. D. McClain, M. Motta, B. Mussard, H. Q. Pham, A. Pulkkin, W. Purwanto, P. J. Robinson, E. Ronca, E. R. Sayfutyarova, M. Scheurer, H. F. Schurkus, J. E. T. Smith, C. Sun, S.-N. Sun, S. Upadhyay, L. K. Wagner, X. Wang, A. White, J. D. Whitfield, M. J. Williamson, S. Wouters, J. Yang, J. M. Yu, T. Zhu, T. C. Berkelbach, S. Sharma, A. Y. Sokolov, and G. K.-L. Chan, Recent developments in the PySCF program package, *The Journal of Chemical Physics* **153**, 024109 (2020).

[66] Q. Sun, T. C. Berkelbach, N. S. Blunt, G. H. Booth, S. Guo, Z. Li, J. Liu, J. D. McClain, E. R. Sayfutyarova, S. Sharma, S. Wouters, and G. K.-L. Chan, PySCF: the Python-based simulations of chemistry framework, *WIREs Computational Molecular Science* **8**, e1340 (2018).

[67] Q. Sun, Libcint: An efficient general integral library for Gaussian basis functions, *Journal of Computational Chemistry* **36**, 1664 (2015).

[68] L.-P. Wang and C. Song, Geometry optimization made simple with translation and rotation coordinates, *The Journal of Chemical Physics* **144**, 214108 (2016).

[69] M. J. Frisch, G. W. Trucks, H. B. Schlegel, G. E. Scuseria, M. A. Robb, J. R. Cheeseman, G. Scalmani, V. Barone, B. Mennucci, G. A. Petersson, H. Nakatsuji, M. Cariati, X. Li, H. P. Hratchian, A. F. Izmaylov, J. Bloino, G. Zheng, J. L. Sonnenberg, M. Hada, M. Ehara, K. Toyota, R. Fukuda, J. Hasegawa, M. Ishida, T. Nakajima, Y. Honda, O. Kitao, H. Nakai, T. Vreven, J. A. Montgomery, J. E. Peralta, F. Ogliaro, M. Bearpark, J. J. Heyd, E. Brothers, K. N. Kudin, V. N. Staroverov, R. Kobayashi, J. Normand, K. Raghavachari, A. Rendell, J. C. Burant, S. S. Iyengar, J. Tomasi, M. Cossi, N. Rega, J. M. Millam, M. Klene, J. E. Knox, J. B. Cross, V. Bakken, C. Adamo, J. Jaramillo, R. Gomperts, R. E. Stratmann, O. Yazyev, A. J. Austin, R. Cammi, C. Pomelli, J. W. Ochterski, R. L. Martin, K. Morokuma, V. G. Zakrzewski, G. A. Voth, P. Salvador, J. J. Dannenberg, S. Dapprich, A. D. Daniels, Ö. Farkas, J. B. Foresman, J. V. Ortiz, J. Cioslowski, and D. J. Fox, Gaussian 09 Revision D.01 (2009).

[70] F. Weigend and R. Ahlrichs, Balanced basis sets of split valence, triple zeta valence and quadruple zeta valence quality for H to Rn: Design and assessment of accuracy, *Phys. Chem. Chem. Phys.* **7**, 3297 (2005).

[71] D. Lemm, G. F. von Rudorff, and A. von Lilienfeld, LERULI.com, Online molecular property predictions in real time and for free, [www.leruli.com](http://www.leruli.com) (2021).

[72] G. Landrum, RDKit (2010).

[73] C. Bannwarth, S. Ehlert, and S. Grimme, GFN2-xTB: An Accurate and Broadly Parametrized Self-Consistent Tight-Binding Quantum Chemical Method with Multipole Electrostatics and Density-Dependent Dispersion Contributions, *Journal of Chemical Theory and Computation* **15**, 1652 (2019).

[74] C. Bannwarth, E. Caldeweyher, S. Ehlert, A. Hansen, P. Pracht, J. Seibert, S. Spicher, and S. Grimme, Extended tight-binding quantum chemistry methods, *WIREs Computational Molecular Science* **11**, e1493 (2021).

[75] C. R. Harris, K. J. Millman, S. J. van der Walt, R. Gommers, P. Virtanen, D. Cournapeau, E. Wieser, J. Taylor, S. Berg, N. J. Smith, R. Kern, M. Picus, S. Hoyer, M. H. van Kerkwijk, M. Brett, A. Haldane, J. F. del Río, M. Wiebe, P. Peterson, P. Gérard-Marchant, K. Sheppard, T. Reddy, W. Weckesser, H. Abbasi, C. Gohlke, and T. E. Oliphant, Array programming with NumPy, *Nature* **585**, 357 (2020).

[76] P. Virtanen, R. Gommers, T. E. Oliphant, M. Haberland, T. Reddy, D. Cournapeau, E. Burovski, P. Peterson, W. Weckesser, J. Bright, S. J. van der Walt, M. Brett, J. Wilson, K. J. Millman, N. Mayorov, A. R. J. Nelson, E. Jones, R. Kern, E. Larson, C. J. Carey, I. Polat, Y. Feng, E. W. Moore, J. VanderPlas, D. Laxalde, J. Perktold, R. Cimrman, I. Henriksen, E. A. Quintero, C. R. Harris, A. M. Archibald, A. H. Ribeiro, F. Pedregosa, P. van Mulbregt, and SciPy 1.0 Contributors, SciPy 1.0: Fundamental Algorithms for Scientific Computing in Python, *Nature Methods* **17**, 261 (2020).

[77] K. Hansen, F. Biegler, R. Ramakrishnan, W. Pronobis, O. A. Von Lilienfeld, K. R. Müller, and A. Tkatchenko, Machine learning predictions of molecular properties: Accurate many-body potentials and nonlocality in chemical space, *Journal of Physical Chemistry Letters* **6**, 2326 (2015).

## SUPPLEMENTARY INFORMATION

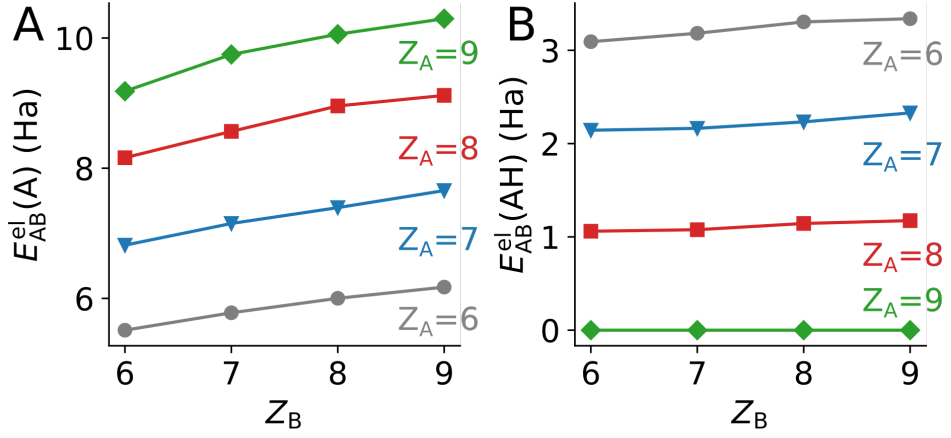


FIG. 8. Atomic electronic binding energies (see Eq. (10)) of atom A as a function of the nuclear charge  $Z_B$  of the binding partner for carbon, nitrogen, oxygen and fluorine (Panel A) and the cumulated atomic binding energies of the hydrogens attached to the different atoms A (Panel B).

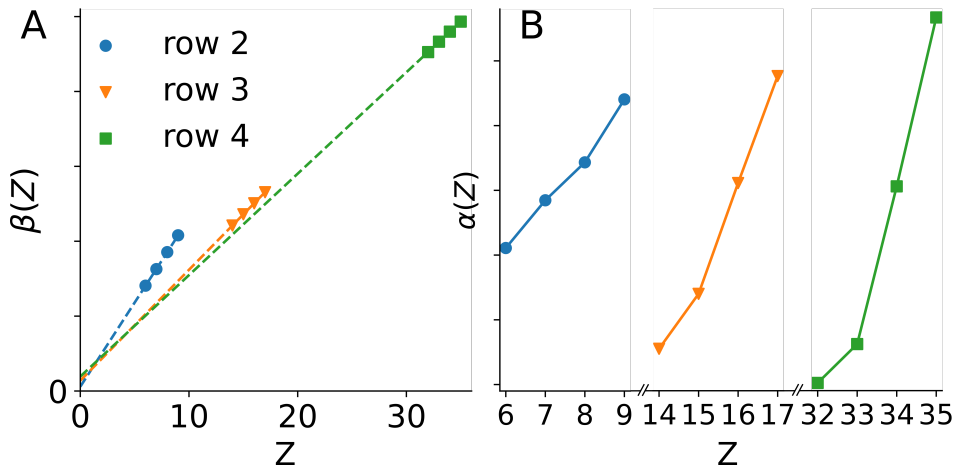


FIG. 9. Optimized parameters  $\beta$  (Panel A) and  $\alpha$  (Panel B) of Eq. (12) as a function of  $Z$  after a fit to binding energies calculated with DFT (PBE0/def2-TZVP).

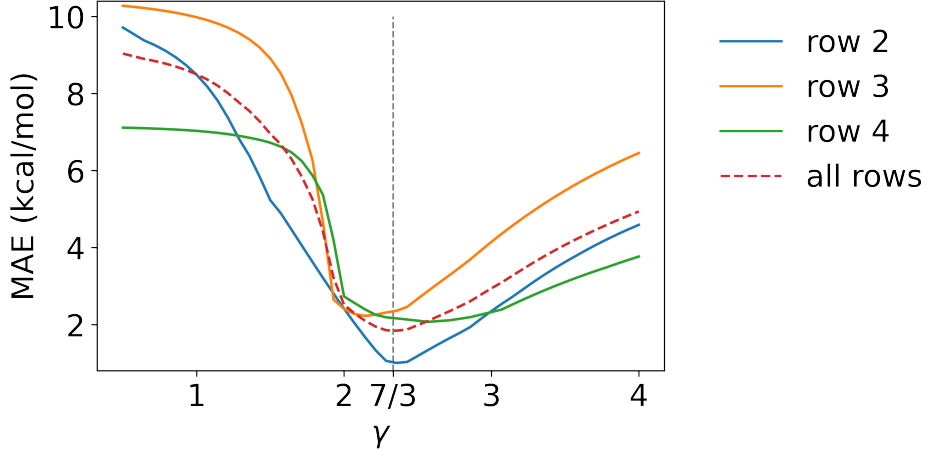


FIG. 10. The mean absolute error for different values of the exponent  $\gamma$  in Eq. (18). The curves labeled row 2, row 3 and row 4 show the MAE if the parameters in Eq. (18) are optimized for each row individually. The dotted red curve shows the MAE for all three rows combined if  $\gamma$  is kept the same for all rows.

TABLE II. The average bond length  $\bar{d}$  of A-B (in Bohr) and the optimized parameters  $(\alpha, \beta)$  for the elements from main group IV to VII for different rows  $n$  of the periodic table. The unit of  $\alpha$  is kcal/mol and  $\beta$  is given as  $630 \cdot ea_0^{-1}$  such that the unit of  $\beta_A Z_A$  is also kcal/mol if  $Z_A$  is provided in atomic units.

$n$	$\bar{d}(a_0)$	IV	V	VI	VII
2	2.69	(55.39, 702.85)	(92.26, 813.36)	(121.54, 926.70)	(170.16, 1039.03)
3	4.01	(-22.70, 1102.97)	(19.71, 1177.84)	(105.29, 1251.12)	(187.89, 1324.77)
4	4.46	(-49.11, 2261.20)	(-19.08, 2330.51)	(102.73, 2397.54)	(233.19, 2464.38)

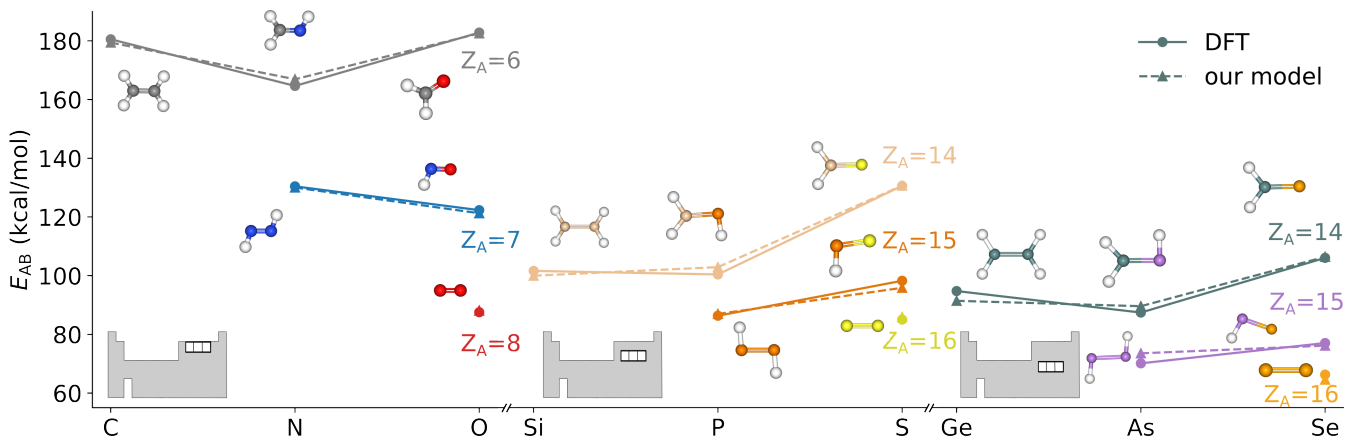


FIG. 11. Calculated bond dissociation energies of double bonds from density functional theory (PBE0/def2-TZVP) and our quantum alchemy based chemical bond model (Eq. (2)). MAEs with respect to DFT amount to 0.9, 1.3 and 2.0 kcal/mol for the second, third and fourth row, respectively.

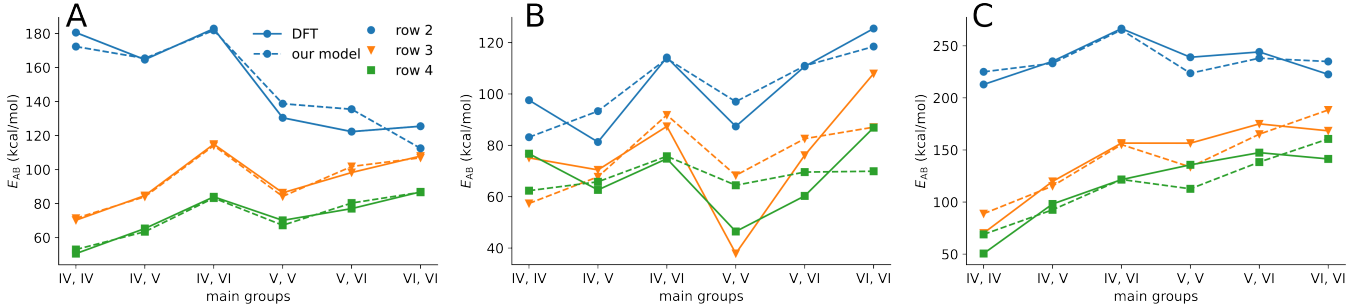


FIG. 12. Energy differences between double bonded molecules  $A=B$  and their fragments  $A, B$  with  $A$  and  $B$  from main groups IV, V, VI in the same row of the periodic table for various electronic states. Predictions are obtained from DFT (PBE0/def2-tzvp) and our model (Eq. (2)). All molecules and fragments are either in their electronic ground state (Panel A), the energetically lowest triplet state (Panel B) or the lowest singlet state (Panel C).

TABLE III. Coefficients and MAEs of our model Eq. (2) for different rows  $n$  after refitting to  $\Delta E^{\text{TS}}$ .  $b$  is scaled such that  $bZ_AZ_B$  is given in kcal/mol if  $Z_A$  and  $Z_B$  are given in atomic units.

$n$	$a$ (kcal/mol)	$b$ (630/ $a_0$ )	$c$ (kcal/mol)	MAE (kcal/mol)
2	439.13	24.3984	4.7284	0.9
3	740.44	18.8836	3.2396	1.3
4	2475.12	14.2104	1.8714	2.0

TABLE IV. Coefficients and MAEs of our model Eq. (2) for different rows  $n$  after refitting to  $\Delta E^{\text{GS}}$ .  $b$  is scaled such that  $bZ_AZ_B$  is given in kcal/mol if  $Z_A$  and  $Z_B$  are given in atomic units.

$n$	$a$ (kcal/mol)	$b$ (630/ $a_0$ )	$c$ (kcal/mol)	MAE (kcal/mol)
2	367.73	19.7386	3.9376	7.4
3	371.53	12.4697	2.2692	1.6
4	874.76	6.7190	0.9318	1.9

TABLE V. Coefficients and MAEs of our model Eq. (2) for different rows  $n$  after refitting to  $\Delta E^{\text{TT}}$ .  $b$  is scaled such that  $bZ_AZ_B$  is given in kcal/mol if  $Z_A$  and  $Z_B$  are given in atomic units.

$n$	$a$ (kcal/mol)	$b$ (630/ $a_0$ )	$c$ (kcal/mol)	MAE (kcal/mol)
2	89.83	6.4716	1.7297	7.3
3	288.38	9.7959	1.7877	13.8
4	758.64	4.8042	0.6495	10.5

TABLE VI. Coefficients and MAEs of our model Eq. (2) for different rows  $n$  after refitting to  $\Delta E^{\text{SS}}$ .  $b$  is scaled such that  $bZ_AZ_B$  is given in kcal/mol if  $Z_A$  and  $Z_B$  are given in atomic units.

$n$	$a$ (kcal/mol)	$b$ (630/ $a_0$ )	$c$ (kcal/mol)	MAE (kcal/mol)
2	333.59	17.6638	4.0305	8.2
3	80.28	8.2754	1.7258	12.9
4	0.00	3.4398	0.5523	12.6

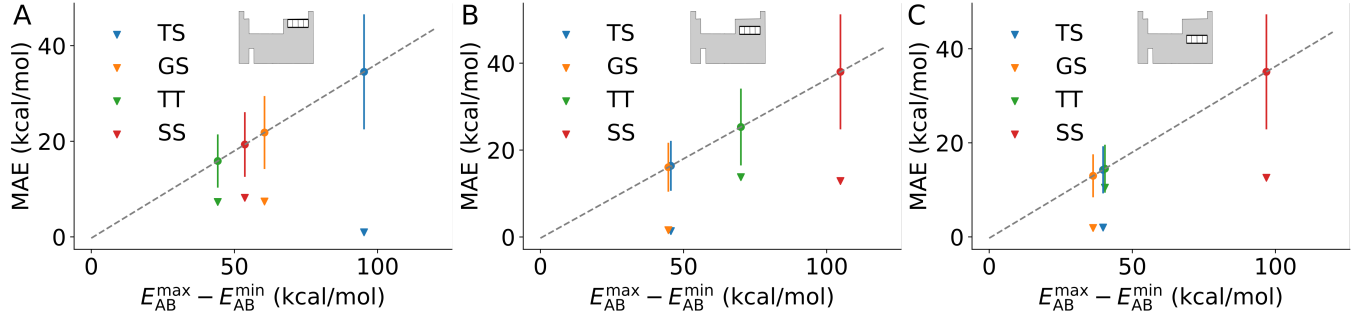


FIG. 13. The performance of our model after re-calibration to binding energy differences of various electronic states in comparison to a fit to random data points from a uniform distribution. Triangles represent MAEs as a function of binding energy range after fitting our model to energy differences between fragments and double bonded molecules as triplets and singlets (TS), in their groundstate (GS), in the lowest triplet states (TT) and the lowest singlet states (SS). The circles with error bars show MAEs and standard deviation after fitting to random data points in the same energy ranges. Panels A, B, C show results for combinations of elements from main groups IV, V and VI for the second, third and fourth row of the periodic table, respectively.